JOURNAL OF Materials CHEMISTRY

Evolution of electronic state, magnetism, and magnetotransport properties in $Sr_3Fe_{2-x}Co_xO_{7-y}$ ($x \leqslant 1$)†

Samrat Ghosh and Peter Adler*‡

Max-Planck-Institut für Festkörperforschung, Heisenbergstr. 1, Stuttgart D-70569, Germany. E-mail: adler@achibm6.chemie.uni-karlsruhe.de

Received 3rd September 2001, Accepted 11th December 2001
First published as an Advance Article on the web 1st February 2002

Iron-rich Ruddlesden–Popper phases $Sr_3Fe_{2-x}Co_xO_{7-y}$ ($x \leqslant 1$) have been synthesized by two citrate precursor techniques and investigated in order to explore the correlation between electron transport properties, electronic state, magnetism, and magnetoresistance effects in iron(IV) based oxides. The materials were characterized by X-ray powder diffraction, temperature and field dependent magnetization measurements, magnetotransport studies, and iron-57 Mössbauer spectroscopy. With increasing cobalt content there is a smooth development of electronic properties: a gradual increase in the low-temperature conductivity of the semiconducting materials, a successive reduction and finally suppression of the charge ordering of $Fe^{(4-\Delta q)+}$ and $Fe^{(4+\Delta q)+}$ sites resulting from a charge disproportionation of the Fe^{4+} ions, and an evolution from antiferromagnetic to ferromagnetic behaviour *via* a spin glass regime. Large magnetoresistance (MR) effects at low temperatures were apparent for all the samples (up to −47% at 5 K and 7 T). Maximization of the MR effects in the title system appears to involve an optimized balance between ferro- and antiferromagnetic interactions.

Introduction

Efforts aiming at understanding and optimizing the colossal magnetoresistance (CMR) properties in perovskite manganites, *i.e.* their extraordinary strong dependence of the electrical resistance on an external magnetic field, have been a frontier topic in solid state and materials science during the last few years.[1–3] It is evident from many studies that the CMR effect involves ferromagnetic metallic-like states competing with insulating para- or antiferromagnetic states. This has also stimulated investigations on the magnetotransport properties of other ferro- and ferrimagnetic perovskite related systems. Examples include the ordered double perovskites $A_2Fe(Mo,Re)O_6$ showing pronounced tunnelling MR effects even at room temperature[4,5] as well as cobalt-based systems.[6]

Recently Battle *et al.* reported for the first time pronounced MR effects in iron(IV) rich oxides, namely the perovskite phases $SrFe_{0.9}Co_{0.1}O_3$ and $Sr_{0.9}Ca_{0.1}FeO_3$.[7] This is particularly remarkable as Fe^{4+} ions, like Mn^{3+} ions which are the main transition metal constituent of many CMR materials, in oxide environment adopt a $t_{2g}^3e_g^1$ high-spin electronic configuration. A maximum MR effect $(R(B)\text{-}R(0)/R(0)) \times 100$ (R denotes the electrical resistance) of −12% at 4 K and 12 T was observed for the metallic cluster-glass system $SrFe_{0.9}Co_{0.1}O_3$. Maignan *et al.* investigated a more extended range of compositions in the system $SrFe_{1-x}Co_xO_{3-y}$.[8] However, the low-temperature MR effects never exceeded values of ∼−10% at 10 K and 7 T. MR effects up to *ca.* −15% at 4 K and 7 T have also been observed for undoped $SrFeO_{2.95}$,[9] where correlations between electrical transport behaviour and magnetic phase transitions are found already in the absence of a magnetic field.

Both, oxygen rich and deficient perovskites $SrFe_{1-x}Co_xO_{3-y}$ reveal high electrical conductivities even at low temperatures. It is well known from the studies on manganites that strong MR effects are favoured in more localized electronic systems. It may then be suggested that the MR effect in Fe(IV) oxides could be enhanced by stronger localization of the metal–oxygen antibonding (σ*) e_g electrons, which can be achieved by reducing the dimensionality of the iron–oxygen network. In addition, incorporation of different amounts of oxygen vacancies into the iron–oxygen network will also have a strong impact on the delocalization of the e_g electrons, the magnetic interactions, and the magnetotransport properties. These pre- sumptions motivated us to investigate the system $Sr_3Fe_{2-x}Co_xO_{7-y}$ the parent compound of which is $Sr_3Fe_2O_7$, the well-known $n = 2$ member of a Ruddlesden–Popper (RP) series.[10–12] Its structure can be described as having layers stacked along the c-axis with two $SrFeO_3$ perovskite slabs separated by SrO rock-salt layers. Indeed, we have found recently a considerably enhanced MR effect of −45% at 5 K and 9 T for $Sr_3Fe_{1.8}Co_{0.2}O_{\sim 7}$,[13] having the same Co content as the perovskite material studied by Battle *et al.* A further interesting feature of this system is that the undoped parent compound reveals a *charge disproportionation* of Fe^{4+} which gives rise to *charge ordering* of electron-rich $Fe^{(4-\Delta q)+}$ (frequently denoted as 'Fe^{3+}') and electron poor $Fe^{(4+\Delta q)+}$ (frequently denoted as 'Fe^{5+}') sites.

In the present paper we report the synthesis of a more extended series of samples in the iron-rich part of the system $Sr_3Fe_{2-x}Co_xO_{7-y}$ ($x \leqslant 1$) by solution-based precursor techniques and comprehensive studies on the properties of this system by powder X-ray diffraction, magnetization and magnetotransport measurements as well as by ^{57}Fe Mössbauer spectroscopy. Emphasis will be put on samples which have been heated under high oxygen pressures for reaching high M^{4+} fractions. However, the effect of oxygen deficiency y on magnetism and magnetotransport properties will be demonstrated for $Sr_3Fe_{1.4}Co_{0.6}O_{7-y}$. From our studies important clues can be drawn about the correlations between chemical composition (Co content x, oxygen deficiency y), electronic state, magnetism, and magnetotransport properties in this system which may turn out to be useful in designing Fe^{4+}-based materials with even stronger MR effects.

During the preparation of this manuscript two other papers

†Electronic supplementary information (ESI) available: additional characterisation data. See http://www.rsc.org/suppdata/jm/b1/b107981f/
‡*Present address*: Institut für Anorganische Chemie, Universität Karlsruhe (TH), Engesserstraße, Geb. 30.45, D-76128 Karlsruhe, Germany.

on the system $Sr_3Fe_{2-x}Co_xO_{7-y}$ have also been published. Prado and Manthiram[14] reported synthesis and some properties of air- and oxygen-annealed samples with $x < 1$ where the M^{4+} contents are smaller than in our materials. No magnetotransport and Mössbauer data were investigated for these oxides. Bréard *et al.* observed a MR effect of −24% at 10 K and 7 T for a Co(IV) rich material, the composition of which was given as $Sr_3FeCoO_{6.94}$.[15] The MR effect is somewhat less but comparable to our previous result in $Sr_3Fe_{1.8}Co_{0.2}O_{\sim 7}$.[13]

2. Experimental

The title oxides were prepared by two solution based precursor routes, *viz*. a citrate–glycerol hybrid gel (CGHG) technique and a matrix trapping and decomposition (MTD) process. The chemicals used were $SrCO_3$ (≥ 99%, Merck), $Fe(NO_3)_3{\cdot}9H_2O$ (≥ 98%, Riedel-deHaën), $Co(NO_3)_2{\cdot}6H_2O$ (≥ 99%, Fluka), $C_6H_8O_7{\cdot}H_2O$ (citric acid, Merck), $C_3H_8O_3$ (glycerol, Merck) and NH_3. The metal contents of both, iron and cobalt nitrates, were determined prior to their use by ICP-AES.

The details of the CGHG process have been given previously.[13] The MTD route is described for $Sr_3Fe_{1.4}Co_{0.6}O_{7-y}$ as a representative. To obtain ∼4 g of the material the following procedure was adopted. In one beaker, 4.69 g of $Fe(NO_3)_3{\cdot}9H_2O$ and 4.88 g of $C_6H_8O_7{\cdot}H_2O$ were dissolved in 50 ml of doubly distilled water. The pH of this brown coloured solution was adjusted to ∼5 by NH_3. The resulting green coloured solution was kept on a magnetic stirrer at room temperature. In another beaker, 26 g of $C_6H_8O_7{\cdot}H_2O$ was dissolved in 100 ml of doubly distilled water and heated. To this solution, 3.67 g of $SrCO_3$ was added gradually, followed by the dissolution of 1.44 g of $Co(NO_3)_2{\cdot}6H_2O$. Thereafter the contents of both beakers were mixed and kept on a water bath maintained at 90 °C with continuous stirring. In the meantime, 100 ashless filter paper circles (589[3] Blue band from Schleicher & Schuell, Ref. No. 300209) of 90 mm diameter were mounted through a perforation at its centre on an alumina rod 150 mm long and 2 mm in diameter. When the solution had been concentrated to almost one-fourth of its original volume, with the help of a dropper, the matrix was quickly soaked with the whole of the viscous solution. After drying the matrix at 100 °C for 1.5 h in a furnace, the alumina rod was placed horizontally on a porcelain trough and was introduced into a preheated Nabertherm PC-S27 furnace at 450 °C. The charring of the matrix and the subsequent calcination in air was carried out under the following conditions: at 450 °C for 2.5 h, (450–900 °C) in 2 h, at 900 °C for 6 h, (900–450 °C) in 6 h followed by rapid cooling to room temperature. The charred product was crushed, compacted in an alumina cylindrical crucible and fired in air at 1000 °C for 24 h. The powder was reground, pelletized and fired in air again at 900 °C for 6 h.

For obtaining samples with high oxygen contents corresponding to high M^{4+} fractions, the pellets derived from the two synthetic routes were annealed under oxygen pressure in an autoclave applying the conditions summarized in Table 1. One batch of air annealed pellets of $Sr_3Fe_{1.4}Co_{0.6}O_{7-y}$ was subjected to flowing oxygen treatment (500 °C, 24 h) in order to obtain increased M^{3+} fractions. The oxygen contents of the products were estimated from iodometric titrations. The materials tend to degrade under prolonged exposure to air.

All samples were characterized by room temperature powder X-ray diffraction (XRD) using a STOE STADI-P powder diffractometer (monochromatic $CuK\alpha_1$ radiation, linear position sensitive detector). Data were collected in Debye–Scherrer mode on samples in a sealed 0.3 mm diameter glass capillary over the range $10° \leqslant 2\theta \leqslant 120°$. Accurate lattice constants were determined from XRD measurements with silicon as an internal standard.

Magnetization measurements as a function of temperature were performed with a SQUID (Quantum Design MPMS 7.0) magnetometer in external magnetic fields of 100 Oe (0.01 T), 10 kOe (1 T), and 70 kOe (7 T). The samples were first cooled down to 5 K without a magnetic field . Subsequently the zero-field-cooled (ZFC) curve was measured by heating to 330 K in the magnetic field. A field cooled (FC) curve was obtained during cooling in the magnetic field. Isothermic magnetization measurements $M(H)$ up to 70 kOe were recorded at various temperatures.

Temperature-dependent ($5 \text{ K} \leqslant T \leqslant 330 \text{ K}$) measurements of the electrical resistivities at 0 and 7 T as well as isothermic magnetoresistance measurements at some temperatures were carried out using the cryostat of a Quantum Design MPMS 7.0 system on rectangular shaped samples (3.8 mm length, 1.5 mm breadth and 1.0 mm thickness) by the four-point contact method. A Keithley 2400 sourcemeter was employed to supply dc currents of up to 1 mA. The voltage drop across the contacts was determined by a HP 34420A nanovoltmeter.

Temperature dependent ^{57}Fe Mössbauer spectra of powdered samples (in the case of high iron contents diluted with polyethylene) were measured in an Oxford flow cryostat with a conventional Mössbauer spectrometer operating with a sine-type drive signal. A $^{57}Co/Rh$ γ-ray source was used for the experiments. The velocity scale was calibrated by measuring the hyperfine splitting of an α-Fe foil. All spectra are referred to α-Fe.

3. Results

3.1. Materials synthesis and structural characterization

In this work single phase samples of $Sr_3Fe_{2-x}Co_xO_{7-y}$ (x = 0, 0.1, 0.2, 0.3, 0.6 and 1.0) could be prepared by two solution based precursor techniques: the CGHG and MTD methods. It turned out that in the CGHG route a corrosion of the quartz beakers occurred which became unusable for further experiments. In the MTD route no quartzware is required and the gelation step is avoided. Molecular mixing of the constituent metal ions is achieved by trapping the metal chelates in the microfibrils of the ashless cellulose matrix. Iodometric

Table 1 Synthesis conditions and oxygen deficiencies for the samples of $Sr_3Fe_{2-x}Co_xO_{7-y}$ studied in this work

x	Synthetic route	Final air annealing[c]	Oxygen annealing	y^h (±0.03)
0	CGHG	1000 °C/24 h	HOP (700–850 bar)[d]	0.09
0.1	CGHG	900 °C/6 h	HOP (700–850 bar)[d]	0.03
0.2[a]	CGHG	900 °C/6 h	HOP (600–700 bar)[e]	0.07
0.3[b]	CGHG	900 °C/6 h	HOP (400–600 bar)[f]	0.29
0.3	CGHG	1000 °C/24 h	HOP (700–850 bar)[d]	0.16
0.6	CGHG	900 °C/6 h	FO[g]	0.40
0.6	MTD	900 °C/6 h	HOP (600–700 bar)[e]	0.20
1.0	MTD	900 °C/13 h	HOP (700–850 bar)[d]	0.28

[a]From ref. 13. [b]This sample was used for MR measurements shown in Fig. 6. [c]Followed by slow cooling to 300 °C and subsequent rapid cooling to room temperature. [d]700 bar at RT → 850 bar at 500 °C for 10 h → 800 bar at 350 °C for 10 h → 700 bar at RT. [e]600 bar at RT → 700 bar at 500 °C for 18 h → 600 bar at RT. [f]600 bar at RT → 600 bar at 500 °C for 18 h → 400 bar (due to pressure leak) at RT. [g]Flowing oxygen (1 bar) at 500 °C for 24 h. [h]Determined from iodometric titrations.

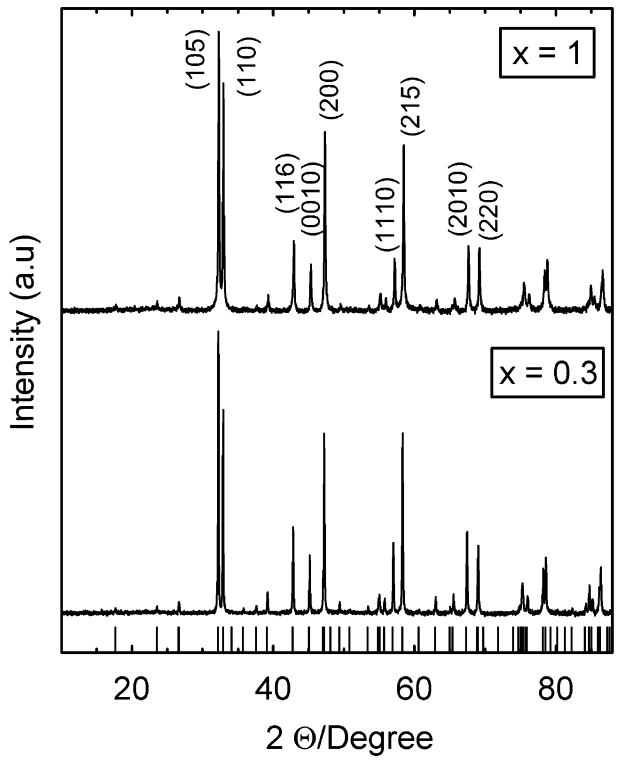

Fig. 1 Representative X-ray powder diffraction patterns of HOP annealed $Sr_3Fe_{2-x}Co_xO_{7-y}$ with $x = 0.3$ and $x = 1$. Miller indices of the most intense reflections are given. Ticks at the bottom indicate the theoretical line positions for the $x = 0.3$ sample.

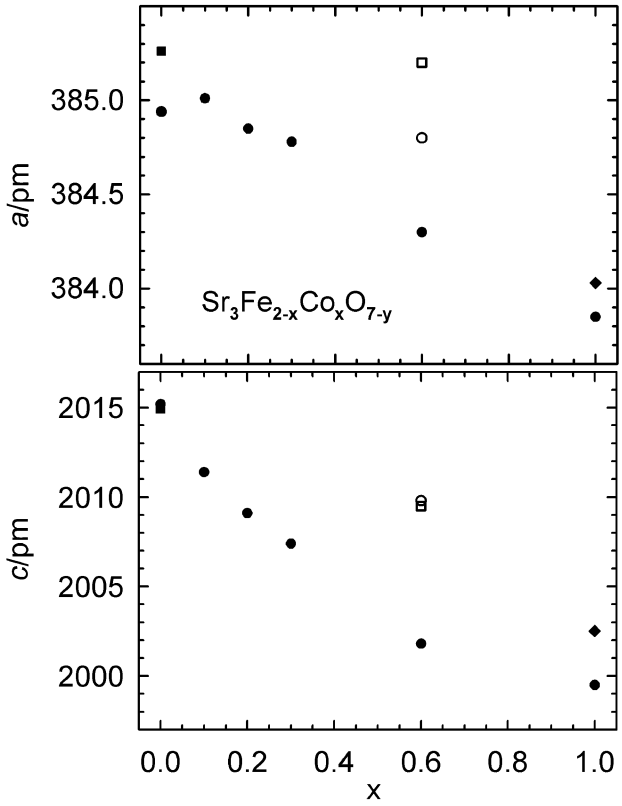

Fig. 2 Lattice parameters a and c of the tetragonal unit cells refined from X-ray powder diffraction data of $Sr_3Fe_{2-x}Co_xO_{7-y}$. Errors are typically < 0.1 pm for the a and < 0.5 pm for the c parameters. Solid circles correspond to HOP annealed samples, the open circle for $x = 0.6$ refers to a FO annealed material. For comparison literature data of HOP annealed $x = 0$,[11] oxygen annealed $x = 0.6$[14] and HOP annealed $x = 1$[15] samples are included (filled squares, open squares, and filled diamonds, respectively).

titrations reveal a certain oxygen deficiency y even for the high oxygen pressure (HOP) annealed samples. The oxygen content on average decreases as the Co content increases. In Table 1 synthesis conditions and oxygen deficiencies are summarized for each sample.

The X-ray powder diffraction patterns of all phases reveal only Bragg reflections expected for the tetragonal space group *I4/mmm* (in Fig. 1 the patterns for $x = 0.3$ and 1 are given as representative). In particular, no additional reflections corresponding to a perovskite phase are seen. For our undoped $Sr_3Fe_2O_{\sim 7}$ reference sample the refined a lattice constant is somewhat smaller than that reported by Weller *et al.*[16] For the HOP annealed samples which according to chemical analysis have high M^{4+} contents (70–95%), the unit cell parameters a and c decrease with increase in the cobalt content (Fig. 2). For flowing oxygen (FO) annealed $Sr_3Fe_{1.4}Co_{0.6}O_{7-y}$ the lattice constants are larger than those for the corresponding HOP annealed material.

3.2 Magnetic and magnetotransport measurements

(a) High oxygen-pressure annealed $Sr_3Fe_2O_{\sim 7}$. In agreement with earlier studies of the parent compound[10–12] the magnetic susceptibility (not shown here) and electrical conductivity ($\sigma = 1/\rho$) curves (see below, Fig. 5) reveal that $Sr_3Fe_2O_7$ is an antiferromagnetic semiconductor ($T_N \sim 120$ K), however with pronounced deviation of the low-temperature conductivity from an Arrhenius-type behaviour. The low-temperature conductivity of the present sample, which was prepared by the CGHG route, is some orders of magnitude smaller than for a previous material synthesized by the ceramic technique.[12] This may reflect certain differences in oxygen content (*cf.* the lattice parameters, Fig. 2) as well as grain boundary effects. The magnetization curve $M(H)$ at 5 K (Fig. 3, top) reveals at first a linear increase of the magnetization M with magnetic field H up to about 30 kOe, but pronounced positive deviations from the low-field straight line above 30 kOe. This is indicative of a ferromagnetic contribution to the exchange interactions. Similar behaviour is observed for other temperatures below T_N. Above T_N, at 130 and 250 K, M increases linearly with H as expected for a paramagnetic system. In Fig. 3 (bottom) the resistance ratio $RR(B) = R(B)/R(0) = \rho(B)/\rho(0)$ is displayed as a function of magnetic flux density B at 10 K. Up to ~ 3 T no MR effect occurs, whereas at higher fields a small albeit significant negative MR effect is apparent. The close correspondence between $M(H)$ and magnetotransport data is noteworthy. At 10 K and 7 T the MR effect $(R(B) - R(0)/R(0)) \times 100$ is about -4%.

(b) High oxygen-pressure annealed $Sr_3Fe_{2-x}Co_xO_{7-y}$. In Fig. 4 the development of the magnetic properties of the system $Sr_3Fe_{2-x}Co_xO_{7-y}$ (HOP annealed) with increasing Co content x is shown (left: temperature dependence of magnetic susceptibilities $\chi = M/H$; right: isothermic magnetization curves $M(H)$, relevant magnetic data for the compounds are summarized in Table 2). As in our previous study for $x = 0.2$[13] it is found that the susceptibility curves are strongly field-dependent. Here, the low-field data at 100 Oe are presented. With increasing x the FC and ZFC maximum susceptibility values increase up to $x = 0.6$, and the shape of the FC and ZFC curves changes considerably. For $x = 0.1$, the FC and ZFC curves show a common sharp maximum at 100 K and the overall behaviour is similar to that observed in the case of undoped $Sr_3Fe_2O_{\sim 7}$[11,12] which is diagnostic of the existence of long range antiferromagnetic order. The latter is progressively disturbed as inferred from the divergence of FC and ZFC curves which becomes prominent as x increases. For $x > 0.2$, both FC and ZFC curves exhibit an inflexion point where there is an abrupt change in $d\chi/dT$. We will refer to the

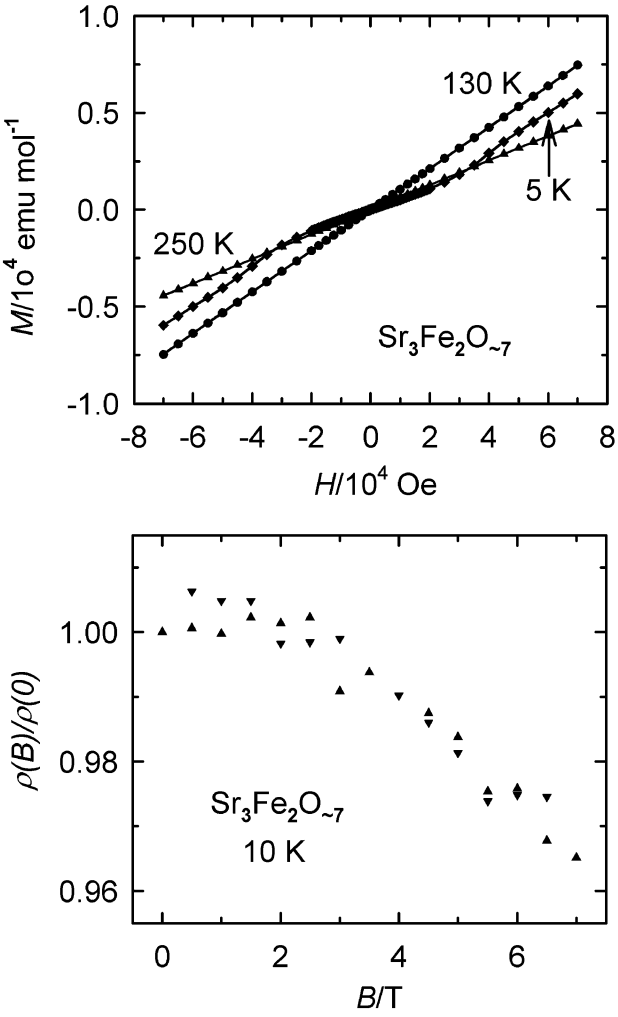

Fig. 3 Isothermic magnetization (top; magnetic moment $M(H)$ as a function of magnetic field H) and magnetoresistance (bottom; resistivity ratio $\rho(B)/\rho(0)$ as a function of magnetic flux density B, triangle up: heating mode, triangle down: cooling mode) data for $Sr_3Fe_2O_{\sim 7}$.

corresponding temperature as T_C. In the vicinity of T_C the FC and ZFC curves show a sharp rise with decreasing temperature. This may indicate a ferromagnetic ordering transition. However, particularly the ZFC curves (*cf.* the data for $x = 0.6$ in Fig. 4) exhibit a complicated behaviour indicating that antiferromagnetic interactions are still of importance. The shift of T_C to higher temperatures with increasing x shows that replacement of iron by cobalt ions leads to strengthening of ferromagnetic interactions. This is in agreement with the trend in the Θ parameters (Table 2) derived from Curie–Weiss fits between 280 and 330 K. In all cases the inverse susceptibilities $\chi^{-1}(T)$ deviate from a straight line showing that $\chi(T)$ does not follow a Curie–Weiss law $\chi = C/(T - \Theta)$ over extended temperature ranges.

The development of pronounced ferromagnetic interactions on Co-doping is also reflected in the isothermic magnetization curves $M(H)$ (see Fig. 4 right). The $M(H)$ curves at 5 K show for all compositions a hysteresis and they become steeper as x increases from 0.1 to 1.0. The parameters characterizing the curves, namely the ordered magnetic moment μ(5 K, 7 T) per magnetic ion at 5 K and 7 T, the coercive field B_C, and the remanent magnetization M_r are also given in Table 2. The following trends are apparent: for quite small x (*e.g.* $x = 0.3$) a pronounced hysteresis with $B_C \sim 0.8$ T develops and μ(5 K, 7 T) increases up to 2.7 μ_B. Higher Co concentrations do not lead to further increase in μ(5 K, 7 T) and B_C decreases again. On the other hand, the M_r(5 K) values increase continuously from $x = 0$ to $x = 1$. Only for $x = 1$ magnetic saturation appears to be reached above 4 T. The $M(H)$ curves at higher temperatures reveal no hysteresis and develop in shape from sigmoidal to linear with increase in temperature.

We now turn to the magnetotransport data. In Fig. 5 the logarithm of the electrical conductivity σ in the absence of a magnetic field is plotted as a function of inverse temperature for the HOP annealed samples. All materials are still semiconducting, however, the conductivities at low temperatures are only weakly activated. Even though the detailed transport properties are also influenced by the oxygen vacancy concentration y, which is not constant for the various materials, overall, the low-temperature conductivity increases by some orders of magnitude from $x = 0$ to $x = 1$. The resistivity values at 5 and 300 K for all the phases are given in Table 3. The development of the magnetotransport behaviour in HOP annealed $Sr_3Fe_{2-x}Co_xO_{7-y}$ is shown in Fig. 6 where the resistance ratios $RR(B)$ are displayed for different temperatures. All the samples show large negative MR effects at low temperatures with MR values between −18 and −35% at 5 K and 7 T (Table 3). The shape of the MR isotherms differs considerably for the various compositions. For $x = 0.1$ pronounced MR effects are only observed above 2 T, whereas with increasing x the $RR(B)$ curves become steeper. The field dependence of the resistance ratios qualitatively reflects the shape of the $M(H)$ curves, as is particularly evident from the hysteresis in the 5 K data. The latter is most pronounced for $x = 0.3$. For the highest Co contents small MR effects are observed even at 250 K ($MR = -2\%$ at 7 T for $x = 1$).

(c) Flowing oxygen annealed $Sr_3Fe_{1.4}Co_{0.6}O_{7-y}$. The magnetization data for FO annealed $Sr_3Fe_{1.4}Co_{0.6}O_{7-y}$ are in good agreement with those reported previously for an oxygen annealed sample with $x = 0.6$.[14] Smaller values for T_C andΘ as well as the shape of the $M(H)$ curves (see Table 2) indicate that ferromagnetic interactions are weaker in the FO than in the HOP annealed compounds. From the electrical transport measurements at 0 T it is observed that the low-temperature conductivity is at least an order of magnitude less than for the HOP sample (Table 3). *However, the MR effect is considerably enhanced in the more oxygen deficient material* (−47% *vs.* −28% at 5 K and 7 T) (Fig. 6).

3.3 Mössbauer spectroscopy

In Fig. 7 low-temperature Mössbauer spectra of the HOP annealed samples of $S_3Fe_{2-x}Co_xO_{7-y}$ are depicted. The spectra are evidence of magnetic ordering, in agreement with the magnetization data. For $x \leqslant 0.3$ the spectra were fitted with a superposition of three six-line patterns A, B, C which correspond to three non-equivalent iron sites. Lorentzian line shapes were assumed, and the intensity ratio within the components of the sextet was restricted to 3:2:1 which is strictly valid in the thin absorber limit. The Mössbauer isomer shifts IS, the hyperfine fields B_{hf}, and the quadrupole interaction parameters ε derived from the fits are summarized in Table 4. It is noted that most of the Mössbauer spectra reveal strong line broadenings which is a consequence of local variations in the environments of the iron atoms due to disorder induced by the substitutions and oxygen vacancies. Actually a distribution of hyperfine interactions occurs.

Considering the oxygen defect concentration y derived from the iodometric titrations (Table 1) and the IS and B_{hf} values, pattern C in the spectra is assigned to Fe^{3+} defect sites. The Fe^{3+} fraction for the $x = 0.3$ sample prepared at 850 bar O_2 (*cf.* Table 1) was only weak and not included into the fits. As for undoped $Sr_3Fe_2O_7$[11,12] the residual spectra for $x \leqslant 0.3$ consist of two sextets with an intensity ratio of about 1:1. As for the parent compound this is evidence for a *charge disproportionation* (CD) of Fe^{4+} resulting in *charge ordering*

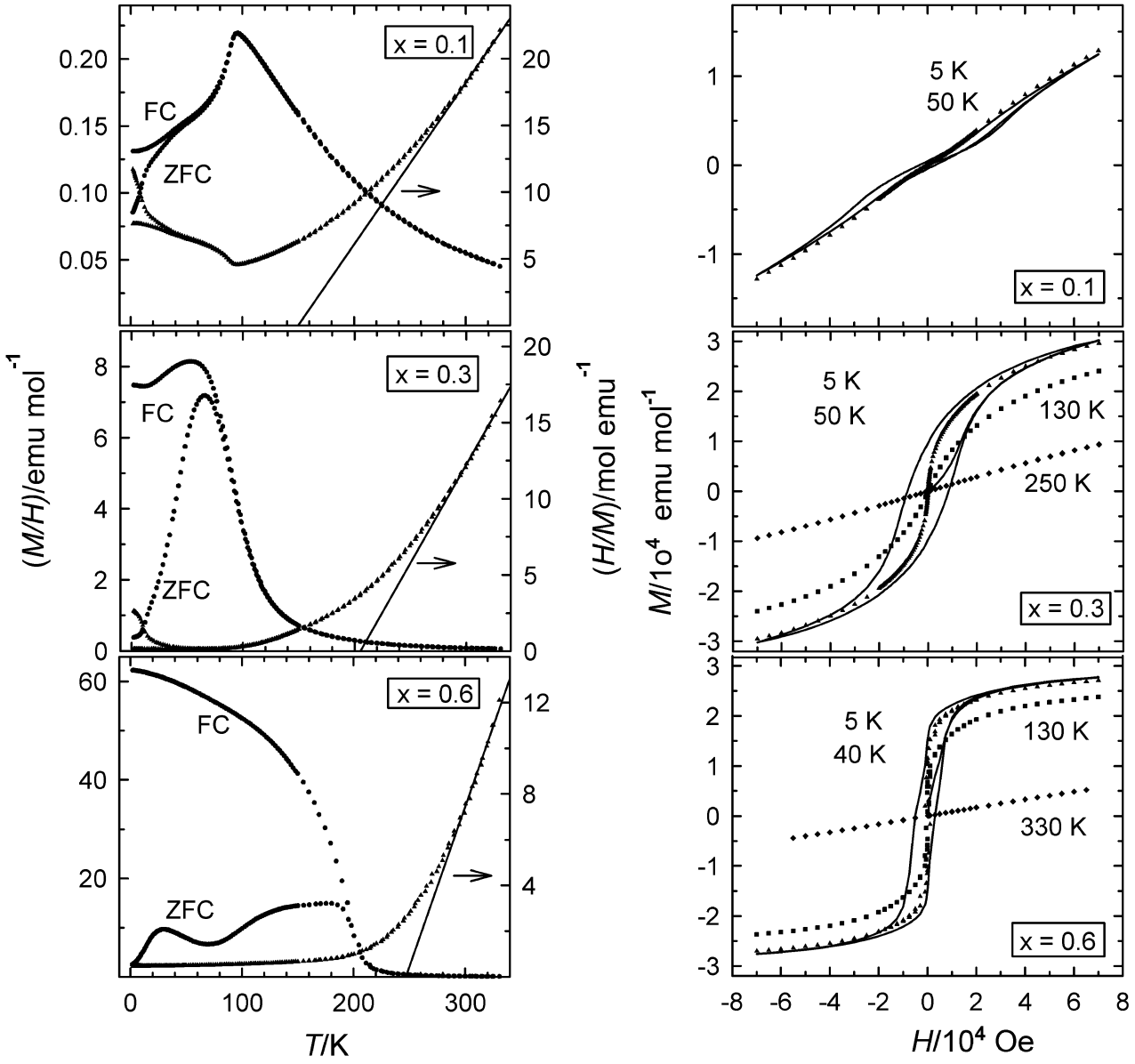

Fig. 4 Evolution of magnetic properties of the system $Sr_3Fe_{2-x}Co_xO_{7-y}$ (HOP annealed). Left: temperature dependence of magnetic susceptibilities $\chi = (M/H)$ and inverse susceptibilities $\chi^{-1} = (H/M)$ at 100 Oe. Right: isothermic magnetization curves $M(H)$. For clarity the hysteresis curves at 5 K are drawn as solid lines.

of electron-poor $Fe^{(4+\Delta q)+}$ (sextet A) and electron-rich $Fe^{(4-\Delta q)+}$ (sextet B) sites. Compared to $Sr_3Fe_2O_7$ there is a considerable decrease in the differences ΔIS in isomer shifts and ΔB_{hf} in hyperfine fields between the two sites with increasing x. In samples with higher levels of Co-doping (x = 0.6, 1) the CD has completely disappeared, and the spectra consist only of one Fe^{4+} and one Fe^{3+} sextet (Table 4).

In Figs. 8–10 the temperature dependence of the Mössbauer

Table 2 Data derived from magnetization measurements on $Sr_3Fe_{2-x}Co_xO_{7-y}$. The effective magnetic moments μ_{eff} and the Θ parameters were obtained from Curie–Weiss fits between 280 and 330 K. Depending on magnetic behaviour characteristic magnetic temperatures are given: Néel temperature T_N for the antiferromagnetic regime, T_C for the more ferromagnetic regime, and a spin freezing temperature T_{sg} for the intermediate regime. T_C is defined by the abrupt increase in the 0.01 T susceptibility curves and does not necessarily imply long range order. The symbols μ(5 K, 7 T), B_C, and M_r(5 K) denote the ordered magnetic moments per magnetic ion at 5 K and 7 T, the coercive field, and the remanence at 5 K, respectively

x, annealing	μ_{eff}(μ_B/ion)	Θ/K	T_C, T_N, T_{sg}/K	μ(5 K, 7 T) (μ_B/ion)	B_C/T	M_r(5 K) (μ_B/ion)
0, HOP	6.01	113	120 (T_N)	0.54	0	0
0.1, HOP	5.75	150	95 (T_N)	1.12	0.35	0.04
0.2, HOP[13]	5.29	189	50 (T_{sg})	1.95	0.80	0.36
0.3, HOP	5.57	205	130 (T_C)	2.70	0.85	0.86
0.3, HOP[a]	5.37	213	140 (T_C)	2.57	0.80	0.86
0.6, HOP	5.35	247	210 (T_C)	2.48	0.50	1.35
0.6, FO	4.61	212	170 (T_C)	2.19	0.65	0.57
1.0, HOP[b]	—	~300	250 (T_C)	2.50	0.20	1.73
1.0, HOP[15]		~260	220 (T_C)	1.75[c]		

[a]Somewhat more oxygen deficient sample used for MR measurements displayed in Fig. 6. [b]Even between 280 and 330 K there is no well defined linear part in $\chi^{-1}(T)$. [c]10 K, 5 T.

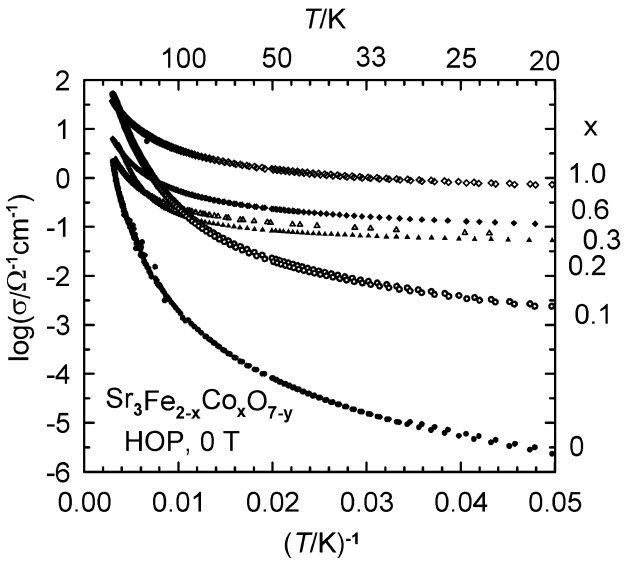

Fig. 5 Logarithm of electrical conductivity $\sigma = 1/\rho$ for HOP annealed $Sr_3Fe_{2-x}Co_xO_{7-y}$ as a function of inverse temperature in the absence of a magnetic field.

spectra for $x = 0.3$ and $x = 0.6$ is shown in detail.[17] The Mössbauer spectra of $Sr_3Fe_{1.7}Co_{0.3}O_{7-y}$ above 100 K are still typical for a paramagnetic phase. Below 100 K line broadening effects are obvious and a magnetic hyperfine pattern starts to develop (*cf.* Fig. 8). The broad features favour an interpretation in terms of relaxation spectra which means that the spin fluctuation rates become comparable to the Mössbauer time scale and decrease with decrease in temperature. Finally, at 7 K a hyperfine pattern is seen which reflects the CD of Fe^{4+}.

Table 3 Electrical resistivities and magnetoresistance effects $MR = (\rho(B) - \rho(0)/\rho(0)) \times 100$ for $Sr_3Fe_{2-x}Co_xO_{7-y}$

x, annealing	ρ(5 K)/Ω cm	ρ(300 K)/Ω cm	MR (%) at 5 K, 7 T
0, HOP[a]	3×10^6	1.0	−4
0.1, HOP	3×10^4	0.03	−28
0.2, HOP[13]	30	0.4	−35
0.3, HOP[b]	27	0.1	−29
0.6, HOP	15	0.2	−28
1.0, HOP	2	0.03	−18
1.0, HOP[15,a]	2×10^2	1.5	−24
0.6, FO	5×10^2	0.5	−47

[a]ρ and MR at 10 K. [b]Somewhat more oxygen deficient sample (*cf.* Tables 1 and 2).

Also in the paramagnetic phase there is still a CD of Fe^{4+} as is apparent from the asymmetric shape of the 150 K spectrum (Fig. 9). Since the spectra are not structured enough for obtaining a unique fit they were modelled by two doublets B and C and one singlet A, corresponding to $Fe^{(4-\Delta q)+}$, Fe^{3+}, and $Fe^{(4+\Delta q)+}$ sites, respectively. The intensity ratio between components A and B was restricted to 1 : 1, taking into account the 7 K spectrum. At higher temperatures the shape of the spectra becomes more symmetric which, similar to our previous studies on $Sr_3Fe_2O_{\sim 7}$[12] and $Sr_3Fe_{2-x}Ti_xO_{7-y}$,[18] indicates that the degree of charge separation is reduced with increasing temperature. It cannot be decided with certainty whether there is still a CD at room temperature. The corresponding spectrum can be reproduced equally well either with

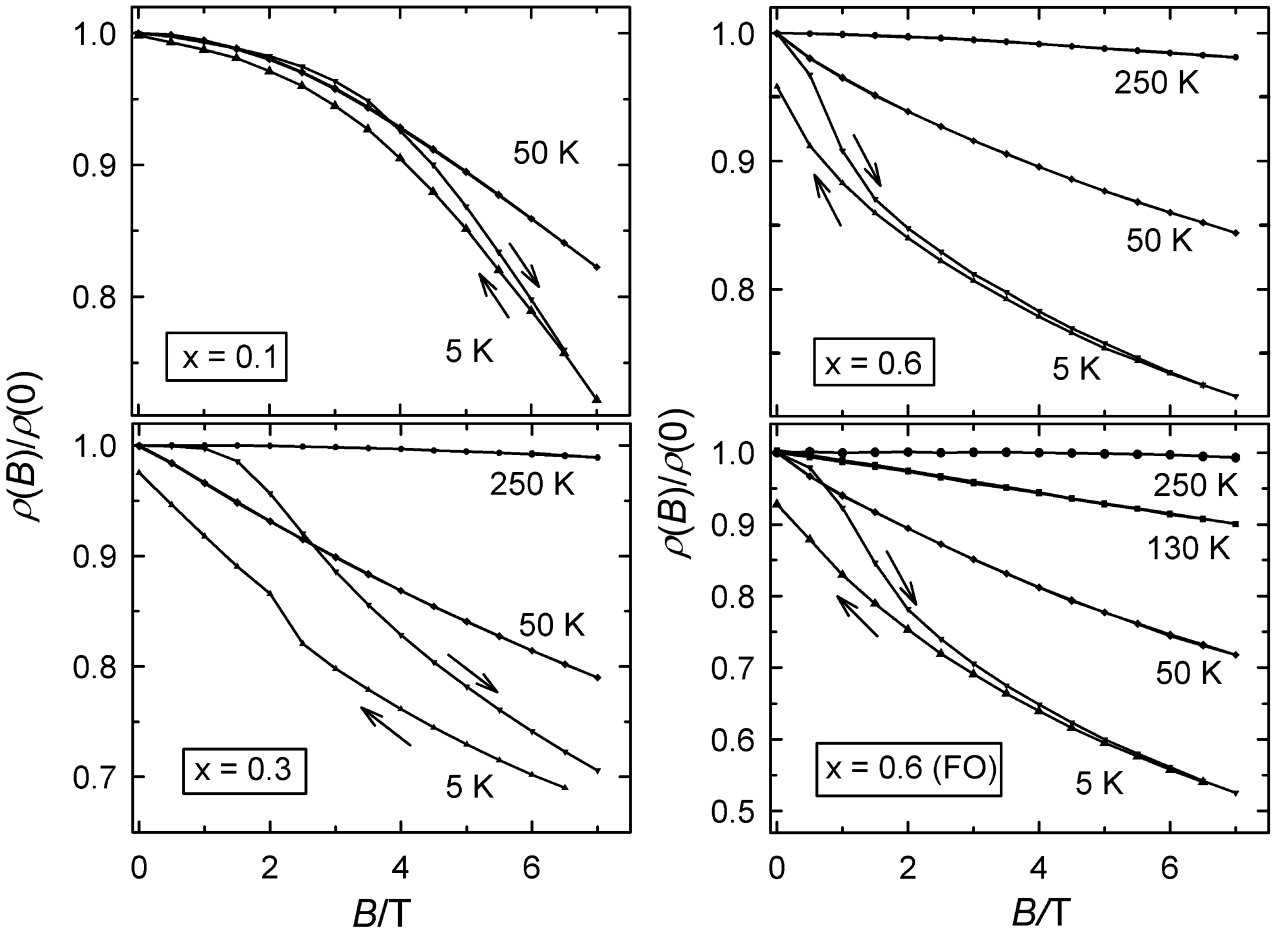

Fig. 6 Isothermic magnetoresistance properties of HOP annealed $Sr_3Fe_{2-x}Co_xO_{7-y}$ and FO annealed $Sr_3Fe_{1.4}Co_{0.6}O_{7-y}$. The resistivity ratios ρ(B)/ρ(0) are displayed *vs.* magnetic flux density B. Solid lines are guides for the eye.

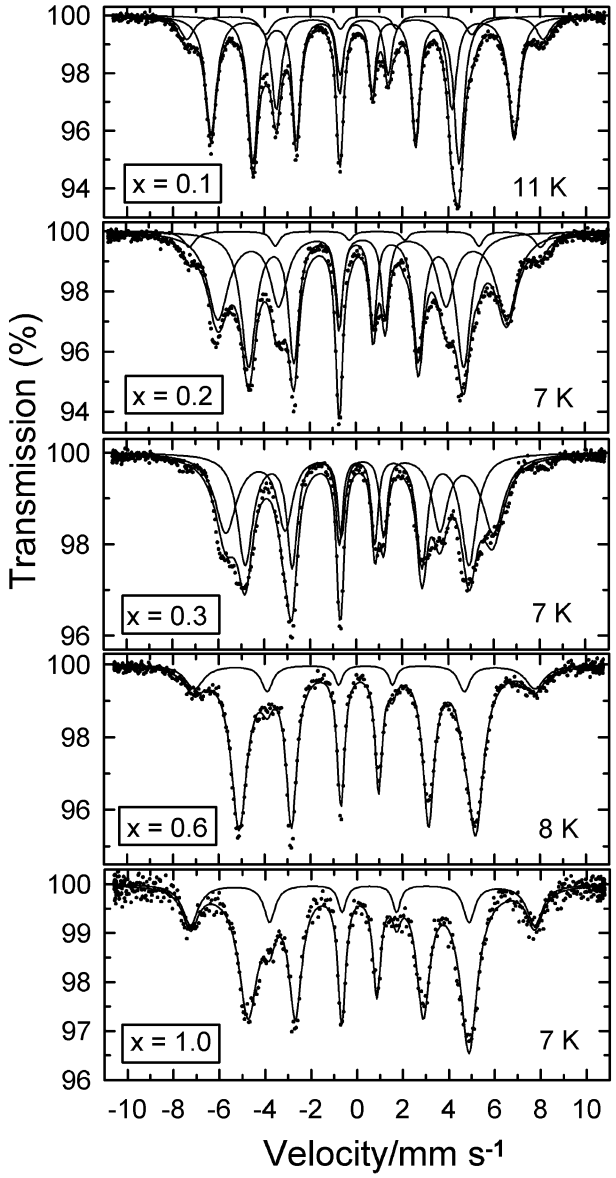

Fig. 7 Low-temperature Mössbauer spectra of HOP annealed $Sr_3Fe_{2-x}Co_xO_{7-y}$, illustrating the development of the electronic state. Solid lines correspond to spectra and subspectra obtained from data fitting.

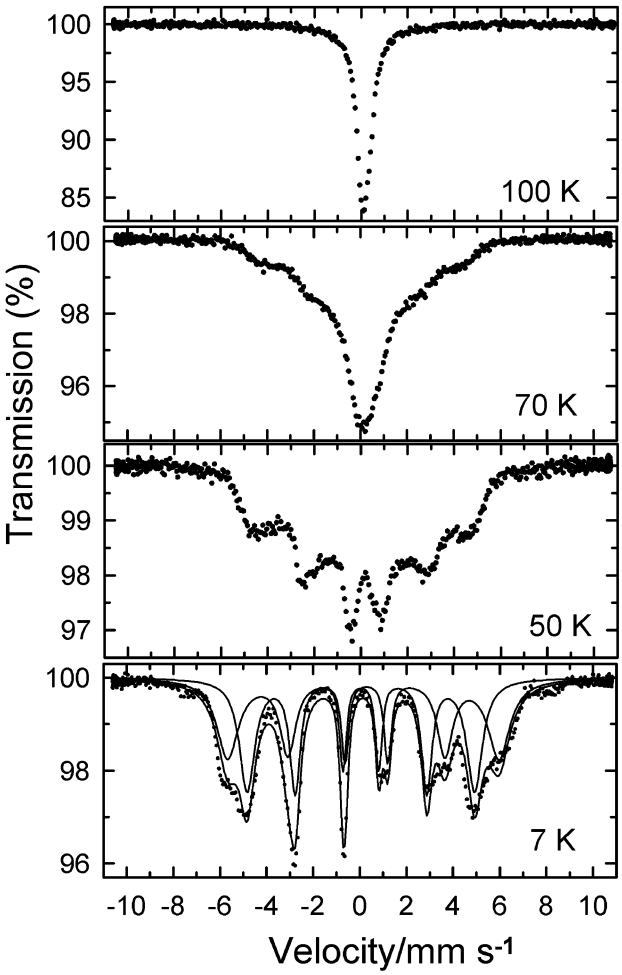

Fig. 8 Temperature dependence of the Mössbauer spectra of HOP annealed $Sr_3Fe_{1.7}Co_{0.3}O_{7-y}$ (850 bar O_2, *cf.* Table 1) illustrating the development of magnetic hyperfine splitting.

the CD model or assuming one Fe^{4+} site with a small quadrupole splitting.

The Mössbauer spectra of $Sr_3Fe_{1.4}Co_{0.6}O_{7-y}$ (Fig. 10) suggest a partial phase transformation to a magnetically ordered phase between 200 and 175 K giving rise to the appearance of a broadened hyperfine pattern in the 175 K spectrum. Most remarkably, the coexistence of paramagnetic and magnetically ordered (MO) phase over a large temperature

Table 4 Mössbauer parameters of HOP annealed $Sr_3Fe_{2-x}Co_xO_{7-y}$ materials at low temperatures. The units are mm s^{-1} for the isomer shifts *IS* and quadrupole interaction parameters ε, and Tesla for the magnetic hyperfine fields B_{hf}. The statistical errors from the fits are <1 in the last digit if not given explicitly in parentheses

Component		$x = 0.1$ (11 K)	$x = 0.2$ (7 K)	$x = 0.3^a$ (7 K)	$x = 0.6$ (8 K)	$x = 1.0$ (7 K)
A	*IS*	−0.02	0.02	0.05	0.10	0.08(1)
	B_{hf}	27.9	29.1	30.3	32.0	29.9(1)
	ε	0[b]	0[b]	0[b]	−0.06	−0.02(1)
	A (%)	43(1)	47(2)	50(3)	85(1)	78(2)
B	*IS*	0.30	0.28(1)	0.22(1)		
	B_{hf}	41.0	39.0(1)	36.2(2)		
	ε	−0.03(1)	−0.02(1)	−0.07(1)		
	A (%)	47(1)	49(2)	50(3)		
B–A	ΔIS	0.32	0.26	0.17		
	ΔB_{hf}	13.1	9.9	5.9		
C	*IS*	0.46(2)	0.46[b]	—	0.38(3)	0.39(3)
	B_{hf}	48.2(2)	48.5(4)	—	46.1(3)	46.6(3)
	ε	−0.08(2)	−0.13(6)	—	−0.02(3)	−0.15(3)
	A (%)	10(1)	5(1)	—[c]	15(1)	22(2)

[a]Sample prepared at higher oxygen pressure (*cf.* Table 1). [b]Parameter not varied. [c]At the detection limit, not taken into account in the data evaluation.

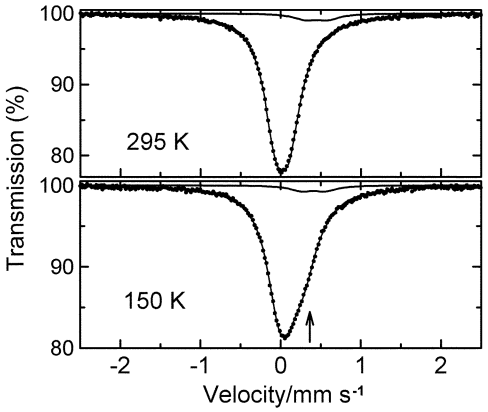

Fig. 9 Mössbauer spectra of HOP annealed $Sr_3Fe_{1.7}Co_{0.3}O_{7-y}$ in the paramagnetic phase. Solid lines correspond to spectra and subspectra obtained from data fitting. For $T = 150$ K a charge disproportionation of Fe^{4+} was assumed. The arrow emphasizes the resulting asymmetric shape of the spectrum. The room temperature spectrum was fitted with one Fe^{4+} and one Fe^{3+} quadrupole doublet.

range is evidenced by Mössbauer spectra recorded between 75 and 175 K. The spectra were reproduced by a superposition of one broadened sextet for the magnetic component and two doublets for the paramagnetic phase. In Fig. 11 the area fractions *A-MO* of the MO phase and *A-Fe*$^{3+}$ of the Fe^{3+} component are depicted as a function of temperature. It is seen that A_{MO} increases gradually below 175 K. In the paramagnetic phase between 75 and 175 K the relative Fe^{3+} fraction is larger in comparison with that in the paramagnetic phase above 200 K. Furthermore, no Fe^{3+} hyperfine sextet is discernible in spectra above 50 K, which indicates that the Fe^{3+} sites do not participate in magnetic ordering for $T \geqslant 50$ K. At 50 K the paramagnetic phase has completely disappeared. However, the Fe^{3+} hyperfine sextet develops only below 50 K (Fig. 11).

4. Discussion

4.1 Chemical and structural properties

In the present study citrate based precursor techniques were used for the synthesis of single phase samples of the system $Sr_3Fe_{2-x}Co_xO_{7-y}$ with $0 \leqslant x \leqslant 1$ at temperatures 900–1000 °C. The advantage of precursor methods lies in the mixing of the metal constituents on a molecular level. In particular, this facilitates the careful control of the metal ratios which is required to prevent formation of other members of the RP series. In a recent report Prado and Manthiram[14] have demonstrated that compositions with $x < 1$ can also be prepared by the ceramic technique at temperatures 900–1300 °C. However, for $x = 1$ an unknown secondary phase was present. Bréard *et al.* used a two-step procedure involving strongly oxygen deficient $Sr_3FeCoO_{6.45}$ for preparing a material, the composition of which was given as $Sr_3FeCoO_{6.94}$.[15]

The results of our iodometric titrations reveal that the oxygen deficiency y of the HOP annealed samples of $Sr_3Fe_{2-x}Co_xO_{7-y}$ on an average increases with cobalt substitution. Similar trends have been observed for air and oxygen annealed samples of $Sr_3Fe_{2-x}Co_xO_{7-y}$ with oxygen annealed phases showing higher oxygen contents than the air annealed ones for fixed x.[14] The more pronounced oxygen deficiency in materials with large cobalt fractions reflects the lower stability of Co^{4+} with respect to Fe^{4+} ions.

Successive replacement of iron by cobalt ions leads to a decrease of the lattice parameters a and c in the case of HOP annealed materials (Fig. 2). By combining the data of ref. 14 with the present ones, it is seen that for a given cobalt content the lattice parameters increase from HOP *via* oxygen to air

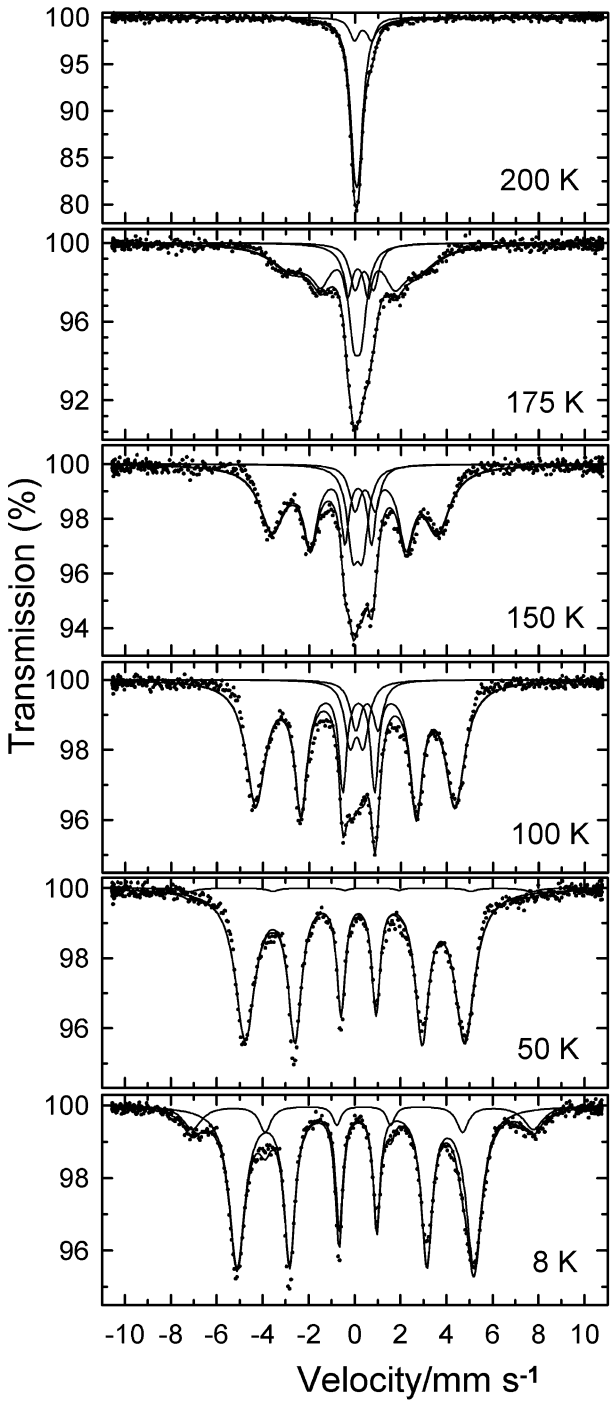

Fig. 10 Temperature dependence of the Mössbauer spectra of HOP annealed $Sr_3Fe_{1.4}Co_{0.6}O_{7-y}$ illustrating the development of magnetic ordering. Solid lines correspond to spectra and subspectra obtained from data fitting (see text for details).

annealed materials, that is with decreasing average oxidation state of the transition metal ion. Two counteracting factors influence the lattice parameters: (a) due to the larger size of M^{3+} ions an increasing M^{3+} fraction results in an expansion of the lattice, and (b) replacement of iron by cobalt ions leads to a contraction of the lattice due to the smaller size of $Co^{4+/3+}$ with respect to $Fe^{4+/3+}$ ions. For the same annealing conditions the latter effect mainly determines the trend in the lattice parameters.

Although the lattice parameter a of the present FO annealed sample with $x = 0.6$ is smaller than that given by Prado and Manthiram[14] for their corresponding oxygen annealed material and c is nearly the same, yet they reported a higher oxygen content (M^{4+} fractions of 60% *vs.* 76%). This may point to

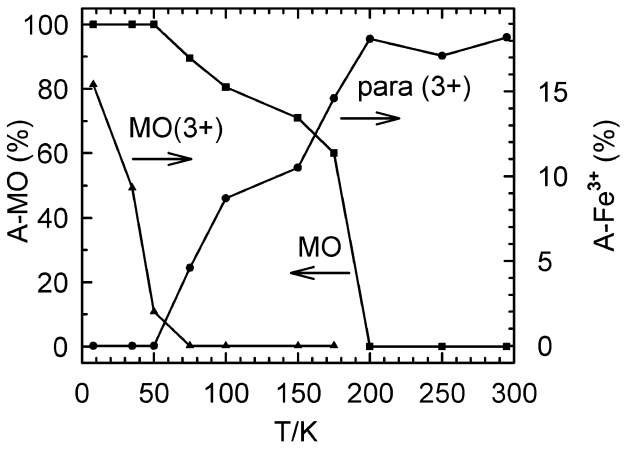

Fig. 11 Temperature dependence of the area fractions derived from the analysis of Mössbauer data of HOP annealed $Sr_3Fe_{1.4}Co_{0.6}O_{7-y}$. *A-MO* and *A-Fe*$^{3+}$ correspond to the magnetically ordered phase, and to the Fe^{3+} species, respectively. Area fractions of the paramagnetic as well as of the magnetically ordered Fe^{3+} sites are shown. Solid lines are guides for the eye.

problems in establishing accurate enough oxygen contents from the iodometric titrations which could also be the reason for unexpected trends when comparing lattice parameters, physical properties (see Section 4.2), and oxygen contents of the present Sr_3FeCoO_{7-y} sample with those from ref. 15. For a given cobalt content the M^{4+} fraction should increase and therefore the lattice constants should decrease with increasing oxygen pressure in the final preparation step. In fact, both lattice constants for the present $x = 1$ sample, which was annealed at 850 bar O_2, are somewhat smaller than those reported by Bréard *et al.* for their sample which was annealed at a lower pressure of 140 bar O_2 (Fig. 2).[15] However, the analytical and Mössbauer data indicate total M^{3+} and Fe^{3+} fractions of 28% and 22%, respectively, for the present material whereas Bréard *et al.* reported a high M^{4+} fraction of 94% for their sample.

4.2 Physical properties

The Mössbauer, magnetization, and magnetotransport measurements described in Section 3 clearly demonstrate the intimate relation between electrical conductivity, electronic state, and magnetic properties in the system $Sr_3Fe_{2-x}Co_xO_{7-y}$. In the case of the HOP annealed samples replacement of Fe^{4+} by smaller Co^{4+} ions leads to strengthening of the covalent M–O–M interactions. This favours delocalization of the σ* antibonding e_g electrons, which explains the observed increase in low-temperature conductivity from $x = 0$ to $x = 1$ by several orders of magnitude (Fig. 5). However all the materials studied here are still semiconducting. The detailed mechanism of the electrical conduction processes remains to be elucidated further as the spin state of the Co^{4+} ions is not clear. Whereas Fe^{4+} ions certainly adopt the $t_{2g}^3e_g^1$ ($S = 2$) high spin configuration, the Co^{4+} ions may either have a t_{2g}^5 low spin ($S = 1/2$), a $t_{2g}^4e_g^1$ intermediate spin ($S = 3/2$) or a $t_{2g}^3e_g^2$ high ($S = 5/2$) spin configuration. Furthermore, the transport properties are complicated by the presence of Fe^{3+} and Co^{3+} ions due to oxygen deficiency even in HOP annealed materials.

In any case, it is obvious from the trends in Mössbauer isomer shifts and magnetic hyperfine fields that the increasing delocalization of the electronic system for small x ($x \leqslant 0.3$) leads to a reduction in the charge and spin separation between the $Fe^{(4+\Delta q)+}$ and $Fe^{(4-\Delta q)+}$ sites resulting from the CD of Fe^{4+} with increasing x. Finally for larger Co contents ($x = 0.6$, 1), corresponding to larger electron delocalization, the CD is completely suppressed, and a single Fe^{4+} site is seen in the Mössbauer spectra. In this respect the present system behaves similar to the distorted perovskite phases $CaFe_{1-x}Co_xO_3$.[19] Replacing Fe^{4+} by Co^{4+} ions has a comparable effect as the application of high pressure on undoped $Sr_3Fe_2O_7$.[20] High pressure strengthens the Fe–O–Fe interactions by decreasing the Fe–O distances which leads to suppression of the CD near 20 GPa. The increased delocalization of the electronic system under high pressures is most evident from an insulator–metal transition above 20 GPa in $Sr_3Fe_2O_7$.[20] The opposite effect, an *increased* charge and spin separation in the CD state has been observed in our previous study of the more localized system $Sr_3Fe_{2-x}Ti_xO_{7-y}$.[18] All these results indicate that the CD state in iron(IV) oxides corresponds to a collective charge- and spin-density wave state in the vicinity of the insulator–metal transition.[12,20] Possibly, the charge ordering of $Fe^{(4+\Delta q)+}$ and $Fe^{(4-\Delta q)+}$ sites involves a structural modulation, which has not yet been directly verified for $Sr_3Fe_2O_7$. However, for the classical CD compound $CaFeO_3$ a distortion attributed to a frozen phonon breathing mode was reported recently.[21,22]

The most prominent effect of Co-doping on the magnetic properties in the system $Sr_3Fe_{2-x}Co_xO_{7-y}$ is the strengthening of ferromagnetic interactions with increasing x. Considering the increased mobility of the electronic system, this is attributed to spin-dependent electron transfer processes, similar to those involved in the double-exchange mechanism in mixed-valent manganites. Delocalization of the e_g electrons causes ferromagnetic interactions *via* Hund's rule coupling to the more localized $t_{2g}(\pi^*)$ electrons. The latter are also the source of competing antiferromagnetic interactions. On going from $x = 0$ to $x = 1$ in the series of HOP annealed materials the balance between antiferromagnetic and ferromagnetic interactions is gradually altered and the system evolves from antiferromagnetism for $x = 0$, 0.1 to ferromagnetic-like ordering for $x = 0.6$, 1. In an intermediate regime ($x = 0.2$, 0.3) the antiferromagnetic and ferromagnetic interactions appear to be of comparable strength which leads to spin frustration effects and spin-glass behaviour. This situation also gives rise to the broad hysteresis in the $x = 0.2$[13] and 0.3 samples. The intimate correlation between electrical and magnetic properties in $Sr_3Fe_{2-x}Co_xO_{7-y}$ is further confirmed by comparing the HOP and oxygen or air annealed samples (present FO annealed material with $x = 0.6$ and data of ref. 14). For a given cobalt content x both the electrical conductivity and the strength of ferromagnetic interactions decrease from HOP *via* oxygen to air annealed materials, *i.e.* with decreasing M^{4+} content. The present material with $x = 1$ reveals somewhat larger conductivities and ferromagnetic interactions than the corresponding sample of Bréard *et al.*[15] (Tables 2 and 3). Similar to the trend in lattice parameters (see Section 4.1) this suggests a somewhat higher M^{4+} content in the present material, which is, however in contradiction to the available analytical and Mössbauer data. Finally it is noted that a development from antiferromagnetism to ferromagnetism was found previously for the corresponding system $SrFe_{1-x}Co_xO_{3-y}$.[23,24] For a given Co content, the Curie temperature for the 3D metallic perovskite phase is significantly higher (*e.g.* $T_C = 350$ K for Sr_2FeCoO_6[24]) than for its 2D analogue in the RP series and hysteresis effects in the $M(H)$ curves are less pronounced.

Additional information about the microscopic mechanism of the magnetic phase transitions in $Sr_3Fe_{2-x}Co_xO_{7-y}$ can be derived from the temperature dependence of the Mössbauer spectra. In the case of small x ($x = 0.2$,[13,17] 0.3) the magnetization measurements indicate ferromagnetic correlations even above 100 K. The absence of a static hyperfine pattern in the Mössbauer spectra at these temperatures suggests the presence of small ferromagnetic clusters, where spin fluctuations are rapid with respect to the Mössbauer time scale. Relaxation spectra at lower temperatures (Fig. 8) indicate a freezing of spins with decreasing temperature. The

spectral shapes are quite similar to those of perovskite-related oxides with spin-glass behaviour[25] which further supports that these systems are magnetically frustrated. For larger x more extended ferromagnetic domains develop which give rise to a magnetic hyperfine pattern in the Mössbauer spectra near 200 K for $x = 0.6$ (Fig. 10) and $x = 1$[17] and to the corresponding steep increase in the magnetic susceptibility curves. The spectra indicate that the Fe^{3+} defects arising from oxygen deficiency are not involved in magnetic ordering in this temperature range. This suggests a microscopic phase separation scenario for explaining the magnetic properties. The ferromagnetic regions develop, driven by the spin-dependent electron transfer processes, only *via* the strongly covalent M–O–M pathways, involving Fe^{4+}, Co^{4+}, and possibly Co^{3+} ions. The electrons of the Fe^{3+} defects are essentially localized and do not participate in the electron-transfer and resulting magnetic ordering processes. Thus regions involving Fe^{3+}–O–M pathways remain paramagnetic. Only at lower temperatures the Fe^{3+} spins become frozen and may couple antiferromagnetically to the ferromagnetic regions.

Coming now to the magnetoresistance properties of the system $Sr_3Fe_{2-x}Co_xO_{7-y}$ it is first noteworthy that the magnitude of the MR effect and its dependence on chemical composition are not as spectacular as for manganites. All Co-doped materials investigated here show quite large MR effects at low temperatures (see Table 3) extending up to nearly -50% at 5 K and 7 T for the FO annealed $x = 0.6$ phase. As conjectured, there is a pronounced enhancement of the MR effect in comparison with the metallic perovskite system $SrFe_{1-x}Co_xO_{3-y}$ where under comparable conditions MR effects of only about -10% were observed.[7,8] Referring to the MR data of HOP annealed $Sr_3Fe_{2-x}Co_xO_{7-y}$ at 5 K (Table 3) it appears that for quite small Co-doping levels the MR effect first increases and becomes strongest in the range $x = 0.2$–0.6, and then decreases again to $x = 1$. Furthermore, it is obvious that the MR effect in the more oxygen deficient FO annealed material with $x = 0.6$ is stronger than in the corresponding HOP annealed sample. Taking into account the development of the magnetic properties these results imply that the maximum MR effect in the system $Sr_3Fe_{2-x}Co_xO_{7-y}$ is achieved by an optimized balance between ferro- and antiferromagnetic interactions. The large MR effects in these materials at low temperatures may then be explained by the favouring of parallel spin alignments at the expense of antiparallel (or more complicated) spin alignments in a magnetic field which facilitates transfer of the e_g electrons. The detailed dependence of the MR effect on chemical composition remains to be further established from studies on more samples with controlled oxygen content. The correlation between magnetic and magnetoresistance properties in $Sr_3Fe_{2-x}Co_xO_{7-y}$ appears to be similar to the system $Sr_2Mo_{1-x}W_xO_6$ where the maximum MR effect was observed for $x = 0.85$, a composition with a spin-glass like magnetism.[26,27]

5. Conclusions

The iron-rich Ruddlesden–Popper (RP) system $Sr_3Fe_{2-x}Co_xO_{7-y}$ ($0 \leqslant x \leqslant 1$) has been synthesized by two citrate-based precursor routes, namely a citrate–glycerol hybrid gel (CGHG) technique and a matrix trapping and decomposition (MTD) process. These materials show an intimate relation between electronic transport properties, electronic state, magnetic behaviour, and magnetoresistance effects. Samples heated under oxygen pressures of 700–850 bar reveal high M^{4+} contents (typically 70–95%, depending on x). This results in a strongly covalent M–O–M network, favouring delocalization of the e_g electrons, which are, however, coupled to the more localized t_{2g} electrons. Increasing the Co content x enhances the charge fluctuations in the e_g subshell with strong impact on the physical properties. In particular, this leads to a suppression of the charge disproportionation of Fe^{4+} and of the resulting charge ordering of electron-rich $Fe^{(4-\Delta q)+}$ and electron-poor $Fe^{(4+\Delta q)+}$ sites, an evolution of the magnetism from antiferromagnetic to ferromagnetic behaviour, as well as to pronounced magnetoresistance effects. Nevertheless, all the present materials are still semiconductors. For higher Co doping levels even stronger oxygen deficient materials show pronounced ferromagnetic interactions. It is remarkable that the largest MR effect (-47% at 5 K, 7 T) in our study was observed in a $x = 0.6$ sample which was annealed in flowing oxygen. The MR effects in the RP series $Sr_3Fe_{2-x}Co_xO_{7-y}$ with a layered crystal structure are strongly enhanced compared to the more ferromagnetic and metallic perovskite series $SrFe_{1-x}Co_xO_{3-y}$.[7,8] Maximization of the MR effects in these iron-based perovskite-related oxides appears to involve an optimized degree of delocalization of e_g electrons and an optimized balance between ferro- and antiferromagnetic interactions.

Acknowledgement

We are grateful to E. Brücher and G. Siegle for performing the large number of magnetic, and magnetoresistance measurements, and to W. Hölle for assistance in the Mössbauer experiments. One of the authors (SG) gratefully acknowledges the grant of a postdoctoral fellowship by the Max-Planck Society.

References

1 A. P. Ramirez, *J. Phys. Condens. Matter*, 1997, **9**, 8171.
2 B. Raveau, A. Maignan, C. Martin and M. Hervieu, *Chem. Mater.*, 1998, **10**, 2641.
3 B. Raveau, M. Hervieu, A. Maignan and C. Martin, *J. Mater. Chem.*, 2001, **11**, 29.
4 K.-I. Kobayashi, T. Kimura, H. Sawada, K. Terakura and Y. Tokura, *Nature*, 1998, **395**, 677.
5 K.-I. Kobayashi, T. Kimura, Y. Tomioka, H. Sawada, K. Terakura and Y. Tokura, *Phys. Rev. B*, 1999, **59**, 11159.
6 A. Maignan, C. Martin and B. Raveau, *J. Supercond.*, 2000, **13**, 313.
7 P. D. Battle, M. A. Green, J. Lago, A. Mihut, M. J. Rosseinsky, L. E. Spring, J. Singleton and J. F. Vente, *Chem. Commun.*, 1998, 987.
8 A. Maignan, C. Martin, N. Nguyen and B. Raveau, *Solid State Sci.*, 2001, **3**, 57.
9 Y. M. Zhao, X. J. Yang, Y. F. Zheng, D. L. Li and S. Y. Chen, *Solid State Commun.*, 2000, **115**, 365.
10 P. K. Gallagher, J. B. MacChesney and D. N. E. Buchanan, *J. Chem. Phys.*, 1966, **45**, 2466.
11 S. E. Dann, M. T. Weller, D. B. Currie, M. F. Thomas and A. D. Al-Rawwas, *J. Mater. Chem.*, 1993, **3**, 1231.
12 P. Adler, *J. Solid State Chem.*, 1997, **130**, 129.
13 S. Ghosh and P. Adler, *Solid State Commun.*, 2000, **116**, 585.
14 F. Prado and A. Manthiram, *J. Solid State Chem.*, 2001, **158**, 307.
15 Y. Bréard, C. Michel, A. Maignan and B. Raveau, *Solid State Commun.*, 2001, **118**, 517.
16 S. E. Dann, M. T. Weller and D. B. Currie, *J. Solid State Chem.*, 1992, **97**, 179.
17 P. Adler and S. Ghosh, Proceedings of the ICAME 2001, Oxford, to be published in *Hyperfine Interactions*.
18 P. Adler, *J. Mater. Chem.*, 1999, **9**, 471.
19 S. Kawasaki, M. Takano, R. Kanno, T. Takeda and A. Fujimori, *J. Phys. Soc. Jpn.*, 1998, **67**, 1529.
20 P. Adler, U. Schwarz, K. Syassen, G. Kh. Rozenberg, G. Yu. Machavariani, A. P. Milner, M. P. Pasternak and M. Hanfland, *Phys. Rev. B*, 1999, **60**, 4609.
21 P. M. Woodward, D. E. Cox, E. Moshopoulou, A. W. Sleight and S. Morimoto, *Phys. Rev. B*, 2000, **62**, 844.
22 T. Takeda, R. Kanno, Y. Kawamoto, M. Takano, S. Kawasaki, T. Kamiyama and F. Izumi, *Solid State Sci.*, 2000, **2**, 673.
23 T. Takeda and H. Watanabe, *J. Phys. Soc. Jpn.*, 1972, **33**, 973.

24 S. Kawasaki, M. Takano and Y. Takeda, *J. Solid State Chem.*, 1996, **121**, 174.
25 P. D. Battle, T. C. Gibb, A. J. Herod, S.-H. Kim and P. H. Munns, *J. Mater. Chem.*, 1995, **5**, 865.
26 K.-I. Kobayashi, T. Okuda, Y. Tomioka, T. Kimura and Y. Tokura, *J. Magn. Magn. Mater.*, 2000, **218**, 17.
27 R. I. Dass and J. B. Goodenough, *Phys. Rev. B*, 2001, **63**, 064417.